ELSEVIER

Numerical study of convective heat transfer from periodic open cavities in a channel with oscillatory throughflow

Toru Fusegi
Engineering Systems International/Nihon ESI K.K., Tokyo, Japan

A numerical study is performed on the fully developed forced-convection heat transfer in a grooved channel with a heated lower plate. Periodic flows are forced through the channel. The time-periodic variations of externally sustained pressure gradients imposed upon the throughflow have significant bearing on the interaction between the throughflow in the channel and the recirculatory flow inside the cavity. Aided by this interaction, convective heat transfer is pronounced for $Re \geq 10^2$, where Re is the oscillatory flow Reynolds number. As the Womersley number increases, the communication between the heated fluid inside the cavity and the throughflow is promoted, leading to heat transfer enhancement. © 1997 by Elsevier Science Inc.

Keywords: heat transfer enhancement; forced-convection; oscillatory flow; grooved channel, finite volume method

Introduction

Heat transfer enhancement has been a major subject of intensive research in thermal engineering. Numerous innovative technological applications rely heavily upon sophisticated heat transfer engineering devices for achieving high performance. For example, integrated circuit (IC) boards with increasing package density and, consequently, higher heat dissipation rates could not operate satisfactorily without effective means of heat removal. Improving the heat transfer performance can be accomplished in such ways as increasing the fan speed, using more powerful cooling agents, and introducing unconventional cooling technologies. Because mechanical constraints existing in the actual device design, cost, and environmental issues, for example, may impose practical limits on the maximum performance of the first two of these options, further progress in cooling technologies awaits the advent of innovative methods. In an effort to augment heat transfer actively, convective heat transfer in oscillatory or pulsatile flows has recently attracted much attention. (The distinction between these two classes of flows is made in the literature based upon the criterion of whether the cycle-averaged flow rate is zero. If so, the flow is oscillatory; otherwise, the flow is said to have pulsatile components about the mean flow rate.)

Since the pioneering study by Sobey (1980), it has been well recognized that much heat and mass transfer enhancement can be expected in corrugated channels using oscillatory flows. Flow patterns accompanying unsteady separation are calculated by Sobey in a sinusoidally furrowed channel. A low-Reynolds number range, in which viscous effects predominate, is considered in his work. He showed that flow separation took place near the upstream side of the wall, resulting in formation of a recirculating cell. This was subsequently ejected into the channel when the throughflow reversed the direction. These features stem from the effects of the streamline curvature caused by streamwise variation in the channel contours. Such effects are absent in a plane channel, for which the heat/mass transfer rate remains constant in the laminar fully developed regime. The vortex dynamics presenting in a corrugated channel promotes mixing of the fluid, leading to heat/mass transfer enhancement.

An extended range of the Reynolds number, including the inertia-dominated regime with highly convective flows, was studied by Nishimura et al. (1991) in a furrowed channel similar to that used by Sobey (1980). The paper described in detail the time-averaged flow pattern, referred to as "steady streaming," that was a manifestation of fluid mixing attributable to vortex dynamics. In both numerical solutions using a finite element method and experimental flow visualization results, time asymmetric flow patterns have been detected wherein the flow fields observable during a half cycle having a positive flow rate differ slightly from those in the negative flow-rate cycle. They appeared in limited ranges of the Reynolds and Strouhal numbers in the inertia-dominated regime. The experimental results demonstrated the onset of three-dimensional (3-D) flows that were thought to be induced by the centrifugal instability arising near the convex surface of the sinusoidally contoured channel walls. Steady streaming, which results from nonlinear interaction between the oscillatory flow and the curved wall, is shown to be a good indicator for measuring of the extent of fluid mixing. For these flows, the possibility of heat/mass transfer augmentation has been confirmed experimentally in a subsequent work, in which the mass transfer rate was measured directly (Nishimura et al. 1993).

In passing, it should be mentioned that heat/mass transfer can be enhanced by applying pulsation to the throughflow. Past work focuses mainly on the behavior of transitional flows for

Address reprint requests to Toru Fusegi, Nihon ESI K.K., 2-47-18 Uehara, Shibuya, Tokyo 151, Japan.

Received 12 March 1996; accepted 25 October 1996

Int. J. Heat and Fluid Flow 18:376–383, 1997

655 Avenue of the Americas, New York, NY 10010

0142-727X/97/$17.00
PII S0142-727X(97)00014-3

which grooves or any object placed in the channel act to induce a hydrodynamic instability. In a grooved-channel geometry, Ghadder et al. (1986a,b) computed self-sustained oscillations, whose characteristics were similar to Tollmien–Schlichting waves, by initially perturbing the throughflow. They found that these excited traveling waves increased the heat transfer rate, which they termed 'resonant heat transfer enhancement."

With a view toward delineating the physical mechanism underlying augmented transport in self-sustained oscillatory flows, Majumdar and Amon (1993) analyzed the kinetic energy equation for the fluctuating components of the flow deduced from direct numerical simulation (DNS) data of the self-sustained oscillatory mode in a communicating channel, which is a two-dimensional (2-D) straight channel with discrete blocks placed at the centerline. They computed the spatial distribution of a *transitional* viscosity ν_{tr}, which was defined for nonturbulent transitional flows in a manner analogous to the turbulent viscosity through the Reynolds stress, and showed that a high concentration of ν_{tr} near the leading and trailing edges of the block was responsible for locally augmenting momentum transport. A similar analysis was undertaken (Kim et al. 1991) for backflows in a channel mounting a single heated block.

Review of the literature presented above reveals that there seems to be little work done for convective heat transfer in a grooved channel with oscillatory throughflow, which is of much relevance to electronic device cooling. Previous investigations in this class of flows focused on the smoothly varying channel shapes, forming a succession of converging–diverging sections so that the throughflow came into contact essentially with the entire flow passage. In contrast, when the surface of the channel embeds rectangular grooves, recirculatory flows appear inside the grooves. Previously, it was found for a grooved channel with nonoscillatory, constant rate throughflow that, for the cavity aspect-ratio (groove height h divided by its width L) $A \geq 0.5$, a standing vortex occupied the entire cavity, preventing the throughflow from contacting the lower heat transfer surface of the groove (Fusegi 1994). Consequently, there is little communication between the throughflow and the inner cavity flow. As long as the viscous effects are strong; i.e., low-Re flows, flow patterns similar to those of nonoscillatory flows persist, even if oscillating throughflow is considered in this geometry (Fusegi 1996). Hence, it is of interest to examine the flow properties in a higher-Re range in search of heat transfer enhancement using oscillatory flow.

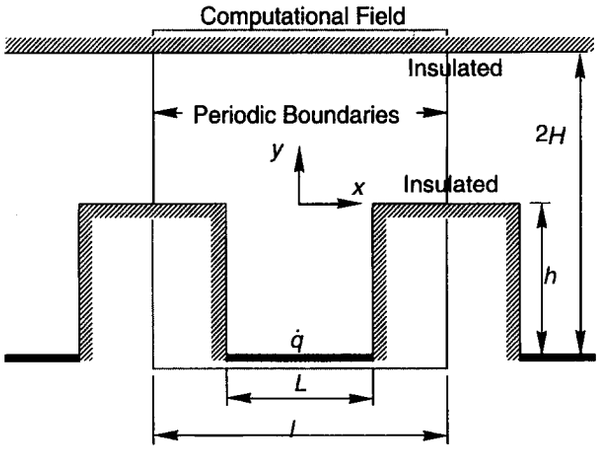

Figure 1 Geometry of the problem and the boundary conditions

In the present investigation, numerical simulations are conducted on convective heat transfer in a 2-D channel between parallel flat plates. The lower plate of the channel is grooved periodically to form open cavities (see Figure 1). The bottom surface of each cavity is heated by a uniform heat flux. The fully developed state of the flow and heat transfer is assumed. This enables us to apply the "periodic condition" in which the field patterns repeat themselves every length of periodicity l. Patankar et al. (1977) presented an appropriate formulation for this class of problems dealing with steady-state fully developed flow and heat transfer by decomposing periodic and nonperiodic parts of variables. It has been extended to an unsteady formulation in an analysis of fully developed oscillatory flow and heat transfer

Notation

c_p specific heat at constant pressure, (J/kg·K)
H half-height of the unobstructed part of the channel (reference length), (m)
h cavity depth, h^*/H
k thermal conductivity of fluid, (W/m·K)
L heated length, (L^*/H)
l length of periodicity, (l^*/H)
$\dot{m}$ mass flow rate per unit span, $(\dot{m}^*/\rho(\Pi/\omega)H)$
Nu Nusselt number, $\dot{q}H/k(\theta_w^* - \theta_b^*)$
$\overline{\text{Nu}}$ average Nusselt number, $L^{-1}\int_{-L/2}^{L/2} \text{Nu}\, dx$
p pressure, $(p^* - p_h)/\rho(\Pi/\omega)^2$, p_h being hydrostatic pressure (N/m²)
Pr Prandtl number, $c_p\mu/k$
$\dot{q}$ heat flux, (W/m²)
Re oscillatory flow Reynolds number, $(\rho(\Pi/\omega)H/\mu)$
Re_m mass flow rate Reynolds number, $\langle\dot{m}^*\rangle/\mu$
St Strouhal number, $[\omega H/(\Pi/\omega)\,(= \text{Wo}^2/\text{Re})]$
t time, ωt^*
u, v velocity components in the x- and y-directions, $[(u^*, v^*)\omega/\Pi]$
Wo Womersley number, $H\sqrt{\omega\rho/\mu}$
x, y Cartesian coordinates, $[(x^*, y^*)/H]$

Greek

β thermal expansion coefficient, (1/K)
Θ parameter defined by Equation 1, $\Theta^* k/\dot{q}$
θ temperature, $(\theta^* k/\dot{q}H)$
θ_b bulk temperature, $\int_0^2 |u|\,\theta\, dy / \int_0^2 |u|\, dy$
μ viscosity, (kg/m·s)
Π parameter defined by Equation 1, (m/s²)
ρ density, (kg/m³)
τ a normalized time, $t/2\pi$
ψ stream function, $\psi^*/H(\Pi/\omega)$
ω frequency of oscillations (1/s)
$\langle\cdot\rangle$ positive half-cycle averaged, $\pi^{-1}\int_0^{2\pi} \max[\cdot, 0]\, dt$ (max$[a, b]$ denotes the larger of the two arguments)

Subscripts

cv at the cavity top, $(y = 0)$
w at the wall

Superscripts

$*$ dimensional quantity

between parallel flat plates by Liao et al. (1994). The same formulation was applied in a previous investigation focusing on mixed convection in a low-Re range by the present author (Fusegi 1996). The mathematical formulation is described below. A simple physical configuration is studied by restricting our attention to single-channel geometry for which the groove is square and set to $h = L = H$ and $l = 2H$. The pressure gradient across the channel varies in sinusoidal form as a function of time. The pertinent dimensionless parameters of the problem are the Reynolds number based on an oscillation velocity scale Π/ω, Re, and the Womersley number Wo. Their definition is provided in the Notation section. These parameters range over $10 \leq \mathrm{Re} \leq 10^3$ and $2 \leq \mathrm{Wo} \leq 2^5$ in the present study. The fluid is air, and the Prandtl number is equal to 0.71.

Mathematical model

Incompressible 2-D flow and heat transfer are assumed throughout. Taking advantage of the periodic boundary condition, pressure P and temperature T are split into periodic components (p and θ) and nonperiodic (linearly varying) parts (Fusegi 1996).

$$P^* = p^* - (\rho \Pi \cos \omega t^*) x^* \quad \text{and} \quad T^* = \theta^* + \Theta^* x^* \tag{1}$$

A variable Θ measuring the energy balance over l is written as follows:

$$\Theta^* = \frac{\dot{q} L^*}{c_p [\dot{m}(t^*)]^* l^*} \quad \text{with} \quad \dot{m}^* \neq 0$$

Note that if $\dot{m}^* = 0$, Θ^* is undeterminable; however, this situation usually does not arise in the numerical computation and, hence, poses no serious problem.

The governing equations for the flow field, after being made dimensionless by selecting H, Π/ω, and ω^{-1} as reference scales for length, velocity, and time, respectively, read

$$\frac{\partial u}{\partial x} + \frac{\partial v}{\partial y} = 0 \tag{2}$$

$$\frac{\mathrm{Wo}^2}{\mathrm{Re}} \frac{\partial u}{\partial t} + \frac{\partial u^2}{\partial x} + \frac{\partial vu}{\partial y} = -\frac{\partial p}{\partial x} + \frac{\mathrm{Wo}^2}{\mathrm{Re}} \cos t + \frac{1}{\mathrm{Re}} \left(\frac{\partial^2 u}{\partial x^2} + \frac{\partial^2 u}{\partial y^2} \right) \tag{3}$$

$$\frac{\mathrm{Wo}^2}{\mathrm{Re}} \frac{\partial v}{\partial t} + \frac{\partial uv}{\partial x} + \frac{\partial v^2}{\partial y} = -\frac{\partial p}{\partial y} + \frac{1}{\mathrm{Re}} \left(\frac{\partial^2 v}{\partial x^2} + \frac{\partial^2 v}{\partial y^2} \right) \tag{4}$$

Moreover, choosing $\dot{q}H/k$ as a reference temperature, the energy equation is expressed as

$$\frac{\mathrm{Wo}^2}{\mathrm{Re}} \left(\frac{\partial \theta}{\partial t} + x \frac{\partial \Theta}{\partial t} \right) + \frac{\partial u\theta}{\partial x} + \frac{\partial v\theta}{\partial y} + u\Theta = \frac{1}{\mathrm{Re} \cdot \mathrm{Pr}} \left(\frac{\partial^2 \theta}{\partial x^2} + \frac{\partial^2 \theta}{\partial y^2} \right) \tag{5}$$

The boundary conditions are prescribed as follows:

$$u = v = 0 \quad \text{at the solid wall (no-slip condition)} \tag{6}$$

$$\begin{cases} \dfrac{\partial \theta}{\partial y} = 1 \quad \text{in} \quad -\dfrac{L}{2} \leq x \leq \dfrac{L}{2} \quad \text{at} \quad y = -h \quad \text{(uniform heat flux)} \\ \dfrac{\partial \theta}{\partial n} = 0 \text{ the normal derivative at the other walls (insulated wall)} \end{cases} \tag{7}$$

$$(u, v, p, \theta)|_{x=1/2} = (u, v, p, \theta)|_{x=-1/2} \quad \text{(periodic condition)} \tag{8}$$

Solution method

The governing Equations 2–5 together with the appropriate boundary conditions, Equations 6–8, are solved numerically using a finite volume method. A nonstaggered grid arrangement, termed the "pressure-weighted interpolation method corrected" (Kobayashi and Pereira 1991), is adapted for the Navier–Stokes equations. In PWIMC, velocities at the control volume faces are evaluated by interpolating adjacent cell center velocities with appropriate weighting, thereby coupling the velocity to the pressure and eliminating nonphysical oscillations in the pressure field. Aside from the collocated grid approach, the present numerical procedure is based on the well-known SIMPLE algorithm (Patankar 1980).

A second-order accurate central difference scheme is employed for the spatial derivatives, except for the convection terms, which are discretized using the third-order QUICK upwind scheme (Leonard 1979). Furthermore, a second-order backward difference formula is applied to preserve overall second-order accuracy in the present solution method. The finite-difference equations are solved sequentially and iteratively within the framework of the fully implicit scheme using the cyclic Tri-Diagonal Matrix Algorithm (TDMA) (Patankar et al. 1977) suitable for the periodic boundaries.

Uniformly spaced meshes are used throughout the calculation field, which is divided by 42×41 grid points in the majority of computations. The time-step is $\Delta t = 0.025\pi$, or equivalently $\Delta\tau = 1/80$, and is found to generate time-step-independent solutions.

Convergence at any time-step is declared when the following criterion is met:

$$\textit{for all grid points and all variables}: \ |\phi^n - \phi^{n-1}|/|\phi^n|_{\max} \leq 10^{-5} \tag{9}$$

where ϕ denotes dependent variables (u, v, p, and θ). The superscripts n and $n-1$ refer, respectively, to the current and previous iteration levels. The developed computer code has been validated by solving standard test problems, for which either exact analytic solutions or highly accurate numerical solutions are available.

The first test problem is the fully developed periodic flow in a plane (ungrooved) channel, which allows a closed form solution. As described in Fusegi (1996), numerical predictions were in excellent agreement with the exact solution. As the second test problem, the fully developed flow with self-sustained oscillations in a grooved channel is considered.

Large-amplitude self-sustained oscillations appear in flows over grooves. The onset of unsteadiness results from the Kelvin–Helmholz hydrodynamic instability of the cavity shear layer. For a periodically grooved channel, the linear stability

analysis was conducted by Ghaddar et al. (1986a) using a spectral–element-based DNS method. Self-sustained oscillations characterized by a time-asymptotic behavior very much like the finite-amplitude Tollmien–Schlichting waves were observed beyond a critical Reynolds number Re_{cr}. Recent finite–difference calculations of a nonlinear analysis that dealt with the full Navier–Stokes equations (Pereira and Sousa 1993) showed results similar to those of Ghaddar et al. (1986a) as to the oscillation characteristics. Both investigations examined the same geometric condition: referring to Figure 1, the geometry of the grooved channel was selected to be $l/H_c = 6.666$, $L/H_c \approx 2.222$, and $h/H_c = 1.111$, where H_c is the half-height of the channel $[H_c = (2H - h)/2]$. In the fully developed state, Re_{cr} (based on H_c and $(3/2)u_m$, u_m being the average velocity) was found to lie within the range of $950 < \mathrm{Re}_{cr} < 1050$, which was substantially lower than that corresponding to an ungrooved channel.

Accurate prediction of the self-sustained oscillatory flow in the grooved channel is a critical test, serving as validation of the present time-dependent solution procedure. In the present computation, the Reynolds number Re_u (defined in the manner described above) was set to 800 and 1200, allowing direct comparison of the results with the previous results (Ghaddar et al. 1986a; Pereira and Sousa 1993). The selected Reynolds numbers encompass the reported $\mathrm{Re}_{cr}(\approx 1000)$. A uniform mesh consisting of 66×31 grid points was used. The initial condition was the plane Poiseuille flow in the upper channel on which Tollmien–Schlichting waves with wavelength of $l/2$ were superimposed. Three time-steps, consecutively refined to be $\Delta t = 0.278$, 0.189, and 0.0947, were used to examine the effect of the temporal resolution. They correspond, respectively, to 1/20th, 1/40th, and 1/80th of the frequency of forced perturbations. By confining our attention to small-amplitude disturbances, the perturbed velocity $\mathbf{v}'$ is written as

$$\mathbf{v}'(x, y, t) = \Re[\hat{\mathbf{v}}(y)\exp i(\alpha x - 2\pi\omega t)]\exp(\sigma t) \qquad (10)$$

where $\hat{\mathbf{v}}$ is the amplitude function, α is the wave number ($2\pi n/l$ with $n = 2$), ω is the frequency, and σ is the amplification rate (a real number). The symbol $\Re[\ ]$ denotes the real part of [ ], and i is the imaginary index. In the linear stability analysis, determination of $\hat{\mathbf{v}}$ amounts to an eigenvalue problem of the well-known Orr–Sommerfeld equation for which $\hat{\mathbf{v}}$, the eigenfunction, is the dependent variable. In a nonlinear analysis, $\mathbf{v}'$ may be arbitrary; nevertheless, $\mathbf{v}'$ given by Equation 10 with $\omega = 0.132$ and $\sigma = -0.02$ is considered in the present computation. This implies that the perturbation will diminish gradually. It becomes ineffective for $t \gg 1$.

Figure 2 shows the time variations of the v-velocity at $x = 0$, $y = 0$ (the midpoint at the upper plane of the cavity) for $\mathrm{Re}_u = 800$ and 1200. Oscillations are damped gradually at $\mathrm{Re}_u = 800$ (a subcritical Re); in contrast, at a supercritical Re_u of 1200, steady oscillations persist, even after the initial disturbance dies down. The obtained frequency is $\omega = 0.147$, which is in good agreement with $\omega = 0.132$ (Pereira and Sousa 1993) and 0.141 (Ghaddar et al. 1986a). For generating the results presented, the smallest time-step ($\Delta t = 0.0947$) was specified. Larger values of Δt reduce the amplitude of oscillations, although the frequency ω remains unchanged.

Results and discussion

Numerical solutions reach periodic states after a few cycles of oscillations, regardless of initial conditions. For convenience of presentation, $t = 0$ is set to the beginning of the periodic states.

Results for low Re ($\lesssim 10$) have been reported elsewhere (Fusegi 1996) and, hence, are only briefly noted here for the sake of completeness. The flow field is characterized by the presence of a standing vortex that fills the whole cavity over almost the entire oscillation cycle. As a consequence, there is little exchange of mass across the upper plane of the cavity ($y = 0$). Heat transfer to the lower wall of the cavity is attributable almost solely to conduction, resulting in low heat transfer rates; i.e., $\mathrm{Nu} \approx 1$. These features are representative of the viscosity dominated flow. In this paper, results for convective flows ($\mathrm{Re} \geq 10^2$) are mainly considered.

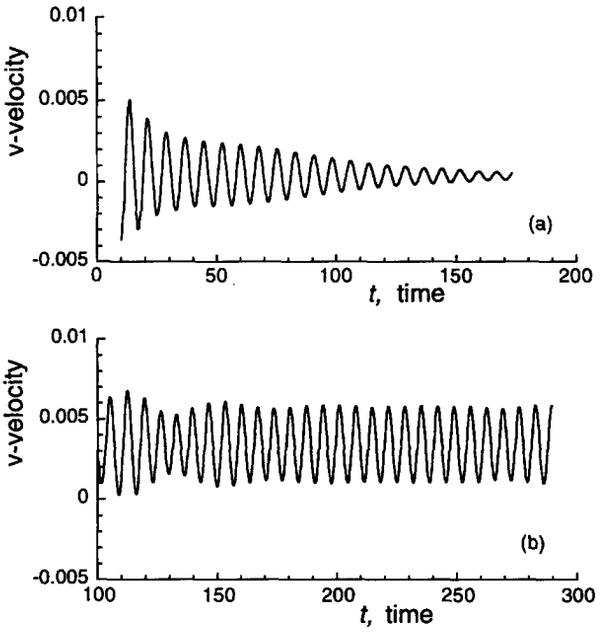

Figure 2 Time history of the v-velocity at $x=0$, $y=0$ (midpoint of the cavity upper plane); (a) $\mathrm{Re}_u=800$, (b) $\mathrm{Re}_u=1200$

Figure 3 shows a series of instantaneous contour diagrams of the flow and temperature fields over a half-cycle at $\mathrm{Re} = 10^2$ and $\mathrm{Wo} = 4$. At every cycle, the pressure gradient reaches the maximum Π and the minimum $-\Pi$ at $\tau = N$ and $N + 1/2$, respectively, where N is integer. In Figure 3a, the streamlines in the throughflow run almost parallel, except for those near the entrance to the cavity, which bend toward the cavity interior. The inner cavity flow is seen to be weak and nearly stagnant. It is noted that, because there is a phase shift between the pressure gradient and the flow rate, as apparent in Figure 6, the flow rate continues to rise until it reaches a peak value at about a time depicted in Figure 3c. Prior to this, a circulatory cell appears in the cavity, as shown in Figure 3b. This vortex grows in size and strength until it merges into the throughflow, when the flow rate approaches zero (Figure 3g). The flow rate turns eventually to negative as the direction of the throughflow reverses, as shown in Figure 3h. During the entire course of these events, the isotherms in the cavity align almost horizontally, which is suggestive of the dominance of conductive heat transfer.

For the rest of the oscillation cycle, during which the pressure gradient changes from the minimum to maximum, the antisymmetric patterns of the above sequence appear (not shown). In contrast, Figure 4, results for $\mathrm{Re} = 10^3$ and $\mathrm{Wo} = 8$, represent convection-dominated features of the oscillatory fields. In Figure 4a, the throughflow forced by the near-maximum pressure gradient is seen to enter the cavity up to about the midheight. This causes the convection of high-temperature fluids upward near the right sidewall. When the pressure gradient decreases, a distinct vortex appears inside the cavity (Figure 4b). From Figures 4c–4g, the vortex wanders inside the cavity by constantly

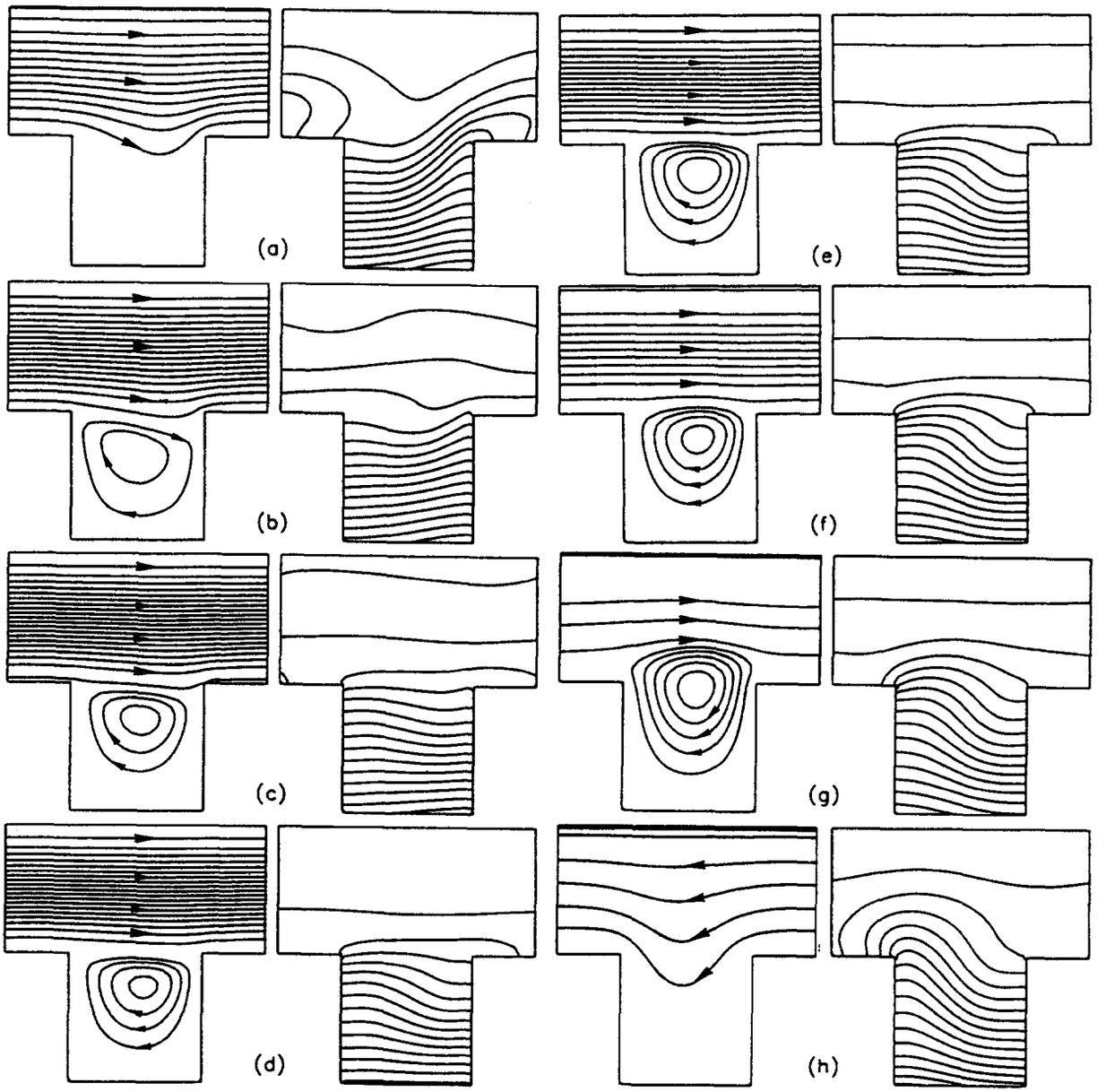

Figure 3 Isovalue contours of the stream function ψ (left) and temperature θ (right) at $Re=10^2$ and $Wo=4$ for a half-cycle of oscillations starting at (a) $\tau=4+1/80$ through (h) $\tau=4+36/80$ with increment of $\Delta\tau=5/80$. [$\Delta\psi=0.037$ (throughflow) and 0.006 (vortex); $\Delta\theta=0.077$]

changing its shape. It is eventually ejected to the channel, as seen in Figure 4h. This vortex circulates heated fluid inside the cavity.

In the remaining half-cycle, the mirror images of the fields depicted here appear, as before. No time asymmetry was detected in the parameter ranges considered in the present investigation.

As elaborated by Nishimura et al. (1991), steady streaming obtainable by time averaging the flow field over the entire oscillation cycle may be regarded as a good indicator of fluid mixing. Figure 5 shows the steady-streaming patterns at the two different Re for $Wo = 4$. In Figure 5a, at $Re = 10^2$, the primary vortex pair is clearly observable in the upper region of the channel where the throughflow is present, and the weaker secondary cells appear inside the cavity. These vortices reflect the existence of rather intense and organized flow patterns in instantaneous flow fields. Because of the large distance from the cavity opening ($y = 0$), the flow in the vicinity of the heated lower plate of the cavity is overall insignificant in this viscosity-dominated flow. In contrast, Figure 5b, depicting the steady streaming at $Re = 10^3$, reveals the tertiary vortex pair near the cavity bottom. The intensity of the secondary vortices is also seen to increase. Because of more prominent inertial effects, the flow in the cavity interior is intensified in this case. When Wo doubles; i.e., $Wo = 8$, the tertiary cells grow in size and come to occupy the larger part of the cavity, responding to an increased penetration depth of the oscillatory throughflow into the cavity (not shown).

Figure 6 shows the time histories of the average Nusselt number $\overline{Nu}$, the mass flow rates of the throughflow $\dot{m}$, and the rate of exchange of the mass flow between the cavity and the channel across the top plane of the cavity ($y = 0$) $\dot{m}_{cv}$. Recalling that the pressure gradient is of cosine function form; i.e., $\cos\tau$, a

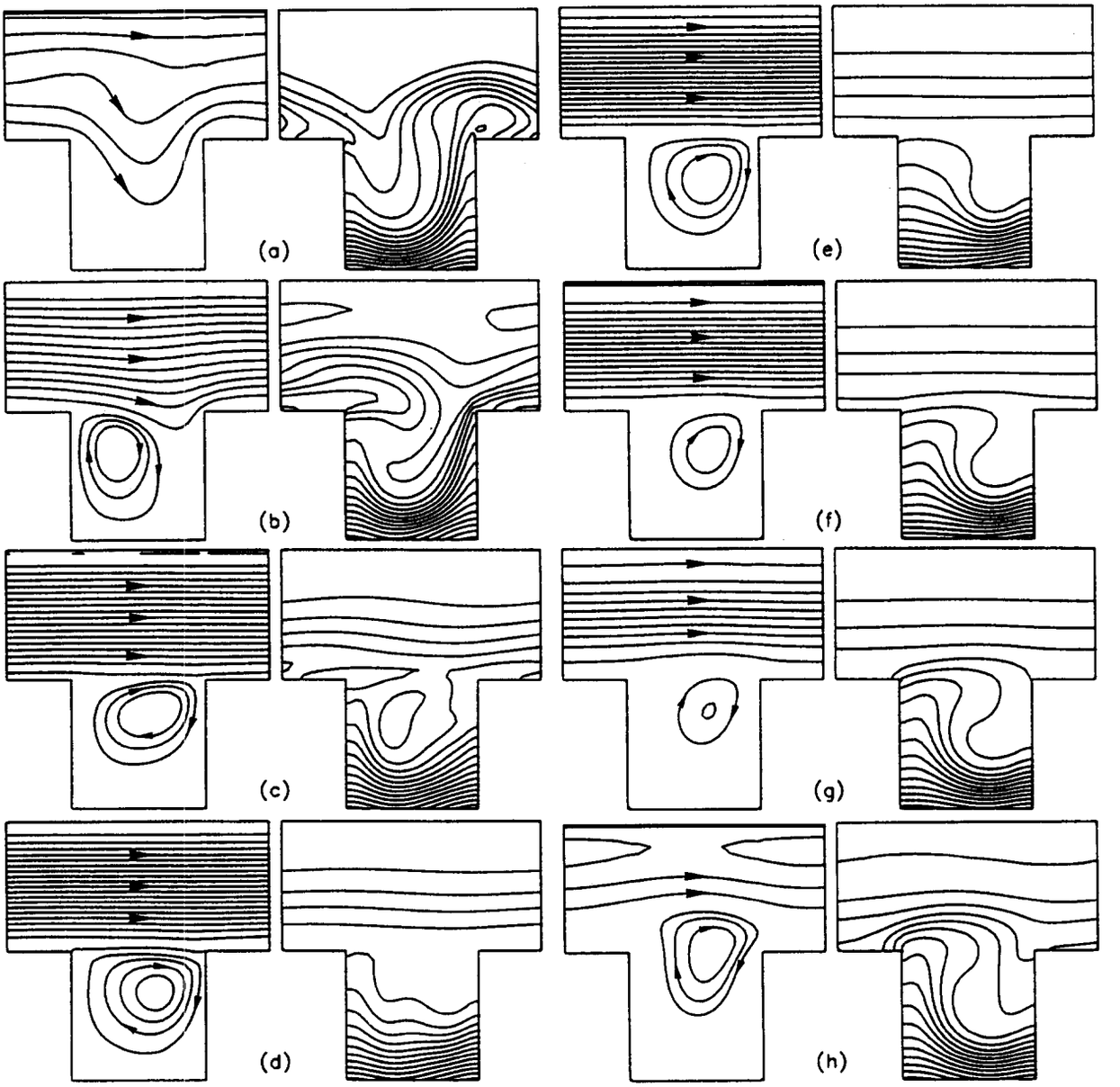

Figure 4 Isovalue contours of the stream function ψ (left) and temperature θ (right) at $Re = 10^3$ and $Wo = 8$ for a half-cycle of oscillations starting at (a) $\tau = 4 + 1/80$ through (h) $\tau = 4 + 36/80$ with increment of $\Delta\tau = 5/80$. [$\Delta\psi = 0.043$ (throughflow) and 0.01 (vortex); $\Delta\theta = 0.031$]

phase shift in $\dot{m}$ is immediately recognizable. It seems to increase for higher Re, suggestive of the intensity of inertial effects. In the heat transfer results, $\overline{Nu}$ values for $Re = 10^2$ and $Wo = 4$ (Figure 6a) are consistently close to 1, because heat transfer is mainly caused by conduction. In contrast, the higher heat transfer rates in Figure 6b (for $Re = 10^3$ and $Wo = 8$) are attributable to the pronounced convection effects. In this case, $\dot{m}_{cv}$ exhibits sharp peaks at every half-cycle of oscillations, reflecting the penetration of the throughflow into the cavity (see also Figure 4a).

Figure 7 is a comprehensive picture of the positive half-cycle-averaged values of $\overline{Nu}$, $\dot{m}$, and $\dot{m}_{cv}$ for the entire ranges of Re and Wo studied in the present investigation. Except for the $\langle\overline{Nu}\rangle$ results in the conduction-dominated cases ($Re \leq 10^2$), these quantities increase monotonically by increasing Re and Wo. For high Re (≥ 500) and Wo (≥ 8), $\langle\overline{Nu}\rangle$ exceeds the value achievable by an unribbed plane channel having nonoscillatory throughflow, as indicated in the same figure. Raising Wo at a given Re leads to an increase in $\langle\dot{m}_{cv}\rangle$ as the throughflow comes to a deeper penetration into the cavity.

Unsteady, aperiodic solutions appeared when Wo was increased further beyond the values considered in the present paper, suggesting the possible existence of flow instability. Because flows may no longer remain 2-D under such situations, no attempt is made in the present investigation to examine this state of flow. This is left as a future work.

Finally, a grid convergence test is reported for the case of $Re = 10^3$ and $Wo = 8$. Table 1 summarizes $\langle\dot{m}\rangle$ and $\langle\overline{Nu}\rangle$ computed using 22×21, 42×41, and 62×61 uniform meshes. As to $\langle\dot{m}\rangle$, the two coarser grid solutions are seen to be within $\pm 1\%$ difference of the fine grid solution. On the other hand, $\langle\overline{Nu}\rangle$ obtained by the coarse 22×21 grids is about 10% lower than

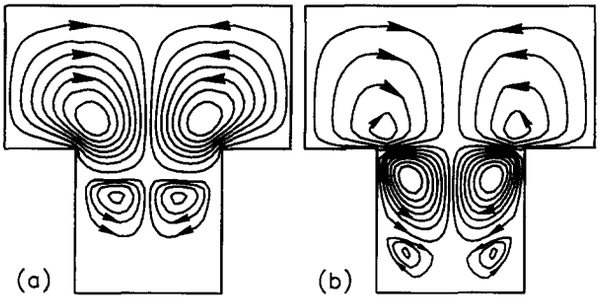

Figure 5 Steady-streaming patterns; (a) $Re=10^2$, $Wo=4$ [$\Delta\psi=8.64\times10^{-4}$ (primary vortices), 8.64×10^{-5} (secondary vortices)]; (b) $Re=10^3$, $Wo=4$ [$\Delta\psi=4.03\times10^{-4}$ (primary vortices); 4.03×10^{-5} (secondary vortices); 4.03×10^{-6} (tertiary vortices)]

that of the fine 62×61 grids. However, $\langle\overline{Nu}\rangle$ of the 42×41 grids agrees with that of the 62×61 grids up to the first three digits. When plotted in Figure 6, the results of the 42×41 and 62×61 grids virtually overlap. Hence, the 42×41 grids are thought to provide sufficiently grid-independent results.

In an effort to provide uniform reporting of grid refinement studies, an index, termed "grid convergence index" (GCI), has been proposed (Roache 1994). The GCI serves as a grid refinement error estimator, which is derived from the generalized Richardson extrapolation. An advantage of the GCI over other error estimators based on the well-known Richardson extrapolation would be that the GCI is conservative, meaning that the actual error (which can be computed if the exact solution exists) is less than an estimated error given by the GCI. The reference (Roache) elaborates on a second-order method applied to two

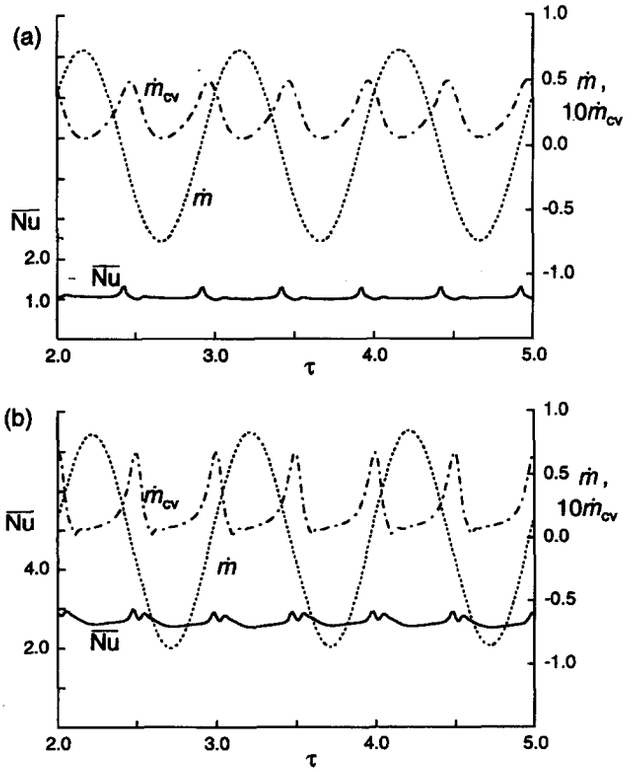

Figure 6 $\overline{Nu}$, $\dot{m}$ and $\dot{m}_{cv}$ versus τ at (a) $Re=10^2$ and $Wo=4$; and (b) $Re=10^3$ and $Wo=8$

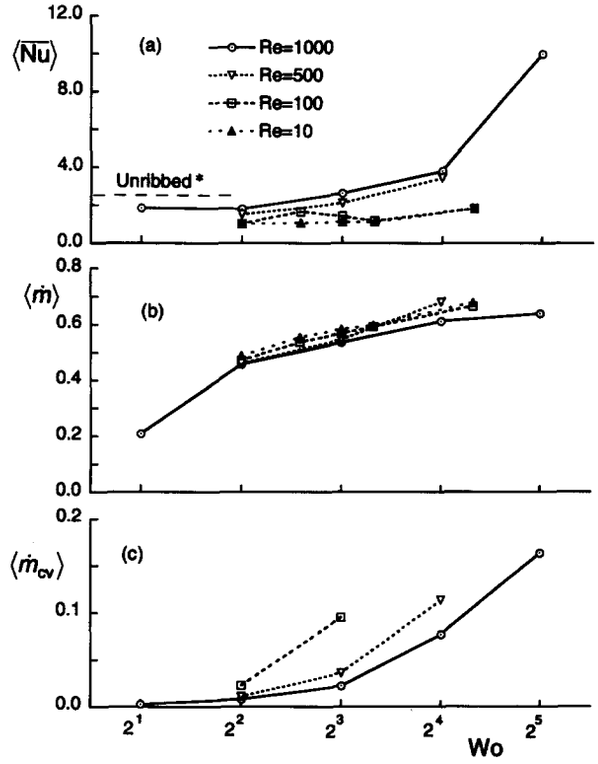

Figure 7 Positive half-cycle-averaged quantities as functions of Wo for various Re; Note: *unribbed channel with nonoscillatory flow ($\overline{Nu}=2.431$, $\dot{m}=2.0$)

sets of finite difference meshes having the uniform grid density (fine and coarse grids). As an attempt to quantifications of an error estimation of the present study, the GCI has been calculated from the $\langle\overline{Nu}\rangle$ data available in Table 1.

Definition of the GCI is (Roache 1994)

$$GCI=\frac{3\cdot|\varepsilon|}{r^p-1} \quad \text{with} \quad \varepsilon=\frac{f_{fine}-f_{coarse}}{f_{fine}} \tag{11}$$

where f_{coarse} and f_{fine} are, respectively, coarse and fine grid solutions, r is the ratio of grid spacing Δ ($\Delta_{coarse}/\Delta_{fine}$), and p is the order of accuracy. The factor 3 is set so that in the case of $r=p=2$; i.e., grid doubling and a second-order method, GCI = $|\varepsilon|$. Note that the normalized actual error may be expressed as

$$\varepsilon_{act}=\frac{f_{fine}-f_{exact}}{f_{exact}}$$

For the present study, f is taken to be $\langle\overline{Nu}\rangle$, an integrated value of the temperature gradient at the bottom wall of the

Table 1 Results of a grid convergence test at $Re=10^3$ and $Wo=8$, showing $\langle\dot{m}\rangle$ and $\langle\overline{Nu}\rangle$ computed using the three difference meshes

	22×21 grids	42×41 grids	62×61 grids
$\langle\dot{m}\rangle$	0.5509 (101%)	0.5372 (99%)	0.5428
$\langle\overline{Nu}\rangle$	2.328 (90%)	2.596 (100%)	2.598

Numbers in parentheses are the percent ratio of the data based on the results of the 62×61 grids.

cavity, and p is set to 2, because the numerical method maintains at least a second-order accuracy. Concerning r, two values are selected; namely, $r_1 = 2\ (= 40/20)$ for the 41 and 21 grids in the y-direction, and $r_2 = 1.5\ (= 60/40)$ for the 61 versus 41 grids. The GCI for these two cases are computed to be $GCI_1 = 10.32\%$ and $GCI_2 = 0.1539\%$. Consequently, a strong grid convergence of the results is indicated between the $(42\times)$ 41 and $(62\times)$ 61 grids.

Conclusions

The properties of oscillatory flows in a periodically grooved channel are studied numerically by systematically varying Re and Wo over extensive ranges. The developed computational procedure was validated by solving the standard test problems dealing with forced oscillatory flow and transitional self-sustained oscillatory flow in a grooved channel. The computed results were compared with the exact solution or with the previously published numerical data. The results demonstrated the ability of the present numerical method to predict the sensitive time-dependent flows accurately.

In the grooved channel with the oscillatory throughflow, the phase shift between the imposed pressure gradient and the flow rate was clearly observed. It is pronounced in high-Re ($> 10^2$) as a manifestation of stronger inertial effects. Communication between the fluid in the cavity, and the throughflow is promoted as Re and/or Wo increase. Particularly in high Wo (≥ 4) studied in the present investigation, the throughflow penetrates deeper into the cavity. This acts to enhance heat transfer to the heated bottom wall of the cavity significantly.

References

Fusegi, T. 1994. Numerical study of mixed convection in a channel with periodic cavities. *Proc. 10th Int. Heat Transfer Conference*, **5**, 471–476

Fusegi, T. 1996. Mixed convection in periodic open cavities with oscillatory throughflow. *Numer. Heat Transfer A* **29**, 33–47

Ghaddar, N. K., Magen, M., Mikic, B. B. and Patera, A. T. 1986a. Numerical investigation of incompressible flow in grooved channels. Part 1. Stability and self-sustained oscillations. *J. Fluid Mech.*, **163**, 99–127

Ghaddar, N. K., Magen, M., Mikic, B. B. and Patera, A. T. 1986b. Numerical investigation of incompressible flow in grooved channels. Part 2. Resonance and oscillatory heat transfer enhancement. *J. Fluid Mech.*, **168**, 541–567

Kim, S. Y., Kang, B. H. and Hyun, J. M. 1994. Convection from a rectangular heated block in pulsating channel flow. *Proc. 10th Int. Heat Transfer Conference*, **4**, 267–272

Kobayashi, M. H. and Pereira, J. C. F. 1991. Calculation of incompressible laminar flows on a nonstaggered, nonorthogonal grid. *Numer. Heat Transfer B*, **19**, 243–262

Leonard, B. P. 1979. A stable and accurate convective modeling procedure based on quadratic upstream interpolation. *Comput. Methods Appl. Mech. Eng.*, **19**, 59–98

Liao, Q. D., Yang, K. T. and Nee, V. W. 1994. An analysis of conjugate heat transfer from a heated wall in a channel with zero-mean oscillatory flow for small oscillatory flow Reynolds numbers. *Int. J. Heat Mass Transfer*, **37** (suppl. 1), 415–423

Majumdar, D. and Amon, C. H. 1993. Physics of heat and momentum transfer in transitional flows in complex geometries. In *Heat Transfer in Turbulent—1993*, R. S. Amano et al. (eds.), HTD, Vol. 246, ASME, New York, 75–83

Nishimura, T., Miyashita, H., Murakami, S. and Kawamura, Y. 1991. Oscillatory flow in a symmetric sinusoidal wavy walled channel at intermediate Strouhal numbers. *Chem. Eng. Sci.*, **46**, 757–771

Nishimura, T., Murakami, S. and Kawamura, Y. 1993. Mass transfer in a symmetric sinusoidal wavy walled channel for oscillatory flow. *Chem. Eng. Sci.*, **48**, 1793–1800

Patankar, S. V. 1980. *Numerical Heat Transfer and Fluid Flow*, Hemisphere, Bristol, PA, Chap. 6

Patankar, S. V., Liu, C. H. and Sparrow, E. M. 1977. Fully developed flow and heat transfer in ducts having streamwise-periodic variations of cross-sectional area. *J. Heat Transfer*, **99**, 180–186

Pereira, J. C. F. and Sousa, J. M. M. 1993. Finite-volume calculations of self-sustained oscillations in a grooved channel. *J. Comput. Phys.*, **106**, 19–29

Roache, P. J. 1994. Perspective: A method for uniform reporting of grid refinement studies. *J. Fluid Eng.*, **116**, 405–413

Sobey, I. J. 1980. On the flow through furrowed channels, Part 1. Calculated flow patterns. *J. Fluid Mech.*, **96**, 1–26